Intracardiac Ultrasound Scanner Using A Micromachine (MEMS) Actuator

Jason M. Zara, Stephen M. Bobbio, Scott Goodwin-Johansson, *Member, IEEE*, and Stephen W. Smith, *Member, IEEE*

Abstract—**Catheter-based intracardiac ultrasound offers the potential for improved guidance of interventional cardiac procedures. The objective of this research is the development of catheter-based mechanical sector scanners incorporating high frequency ultrasound transducers operating at frequencies up to 20 MHz. Our current transducer assembly consists of a single 1.75 mm by 1.75 mm, 20 MHz PZT element mounted on a 2 mm by 2 mm square, 75 μm thick polyimide table that pivots on 3-μm thick gold plated polyimide hinges. The hinges also serve as the electrical connections to the transducer. This table-mounted transducer is tilted using a miniature linear actuator to produce a sector scan. This linear actuator is an integrated force array (IFA), which is an example of a micromachine, i.e., a microelectromechanical system (MEMS). The IFA is a thin (2.2 μm) polyimide membrane, which consists of a network of hundreds of thousands of micron scale deformable capacitors made from pairs of metallized polyimide plates. IFAs contract with an applied voltage of 30–120 V and have been shown to produce strains as large as 20% and forces of up to 8 dynes. The prototype transducer and actuator assembly was fabricated and interfaced with a GagePCI analog to digital conversion board digitizing 12 bit samples at a rate of 100 MSamples/second housed in a personal computer to create a single channel ultrasound scanner. The deflection of the table transducer in a low viscosity insulating fluid (HFE 7100, 3M) is up to $\pm 10°$at scan rates of 10–60 Hz. Software has been developed to produce real-time sector scans on the PC monitor.**

I. Introduction

CATHETER-BASED intravascular ultrasound (IVUS) has had success in the imaging of the vascular system and has received significant attention in past years [1–3]. However, due to the large lumens and asymmetric geometry of the heart, the conventional circular side-scanning geometry of these probes may be less suitable for some cardiac applications. Attempts have also been made to develop forward viewing IVUS transducer probes [4], [5]. More recently, intracardiac ultrasound has become important. Procedures that would benefit from intracardiac guidance include endocardial electrophysiological (EP) mapping, valve repair and replacement procedures, repair of atrial and ventricular septal defects, and radio frequency (RF) ablation for the treatment of cardiac arrhythmias [6]. Several different approaches are being taken in the development of intracardiac ultrasound probes. These approaches include the use of traditional intravascular circular side scanning probes in the heart that operate at frequencies of 12.5–20 MHz [6], side-viewing sector phased array probes that operate at frequencies between 5 and 10 MHz [7], curvilinear array probes that operate at a frequency of 8 MHz (EP MedSystems, Mt. Arlington, NJ), and both side-viewing and forward-looking two-dimensional arrays that produce three-dimensional pyramidal scans and operate at frequencies of 5–7 MHz [8], [9]. In this paper we describe a forward-looking, single-channel mechanical sector scanner that operates at a frequency of 20 MHz.

Intracardiac ultrasound would have advantages over fluoroscopy for the guidance of interventional cardiac procedures, including improved soft tissue contrast and an ability to directly visualize tissues during EP mapping and to continually monitor the RF ablation process [10]. As an example, in order to examine the ability of a high frequency ultrasound probe to image ablated cardiac tissues, we performed an in vitro RF ablation procedure using excised sheep myocardium. As shown in Fig. 1, unfixed, excised sheep myocardium was ablated with a commercially available RF ablation system then imaged using a 20 MHz PZT transducer that was linearly translated across the ablated area of the tissue. The myocardium then was sectioned along the line of the ultrasound scan and photographed to provide a comparison. These experiments produced results similar to those of Kalman *et al.* [11]. The ultrasound image shows that the ablated areas have an increased echogenicity compared to normal tissue at this imaging frequency. This procedure would allow electrophysiologists to not only visualize in real-time where in the heart the RF ablation was conducted, but also to determine the extent to which the tissue has been ablated.

Both forward-looking and side-viewing devices have potential intracardiac applications. Fig. 2 depicts the use of a probe in these two ways. For example, a forward-looking probe could image sites of electrophysiological arrhythmias. The probe could be inserted into the right atrium to image the os of the coronary sinus near the tricuspid valve [10]. Alternatively, the probe could be advanced into the left atrium via a septal puncture from the right atrium

Manuscript received March 25, 1999; accepted January 25, 2000. This work was supported in part by HHS GrantHL-58754, CA-56475, NSF ERC-8622201.

J. M. Zara and S. W. Smith are with the Department of Biomedical Engineering, Duke University, Durham, NC 27708 (e-mail: jzara@duke.edu).

S. M. Bobbio is with the Department of Electrical and Computer Engineering, UNC-Charlotte, Charlotte, NC 28223.

S. Goodwin-Johansson is with MCNC, Electronic Technologies Division, Research Triangle Park, NC 27709.

0885-3010/$10.00 © 2000 IEEE

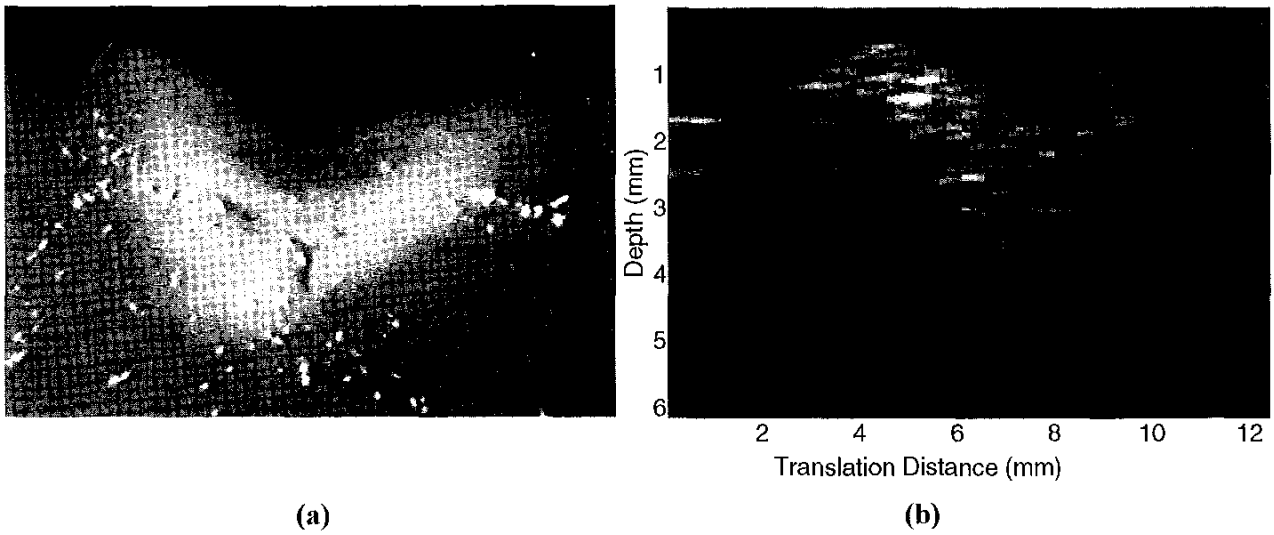

Fig. 1. In vitro RF ablation results, (a) Photograph of sectioned RF ablated sheep heart tissue, (b) 20 MHz translational image of ablated sheep heart tissue.

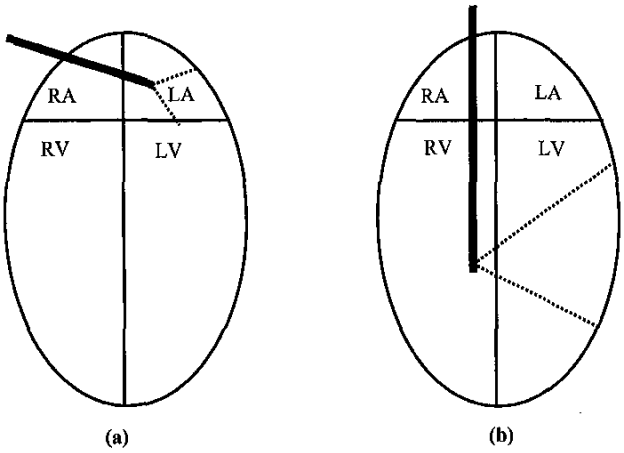

Fig. 2. Diagram of possible usages of (a) the forward looking probe, and (b) the side viewing probe.

to image the vicinity of the pulmonary veins [2(a)]. These areas are believed to be important sites for conduction abnormalities that can lead to atrial arrhythmias; therefore, they are important locations for endocardial mapping and RF ablation procedures. In addition, a side-viewing device could be inserted into the right ventricle from the right atrium via the tricuspid valve, and then could scan through the ventricular septum into the left ventricle. The imaging of the left ventricle could be used to continuously monitor ventricular contraction in cardiac intensive care patients.

We previously described a potential design for a side-viewing scanner [12], [13], but its development has not yet been completed. To this point, we have developed and tested a new type of forward-looking intracardiac probe. The device consists of a single PZT element mounted on a polyimide table resting on flexible polyimide hinges. An integrated force array (IFA) actuator, which is a micromachine (i.e., a microelectromechanical system (MEMS) device) is then used to tilt the transducer in order to create a forward-looking sector scan. The IFA can be driven at AC frequencies (10–60 Hz) to create real time sector scan images. In this paper we describe the prototype design, fabrication, and testing of this intracardiac ultrasound probe. We hypothesize that, with this novel approach to the problem, we will be able to develop a device that will provide high resolution forward-looking ultrasound images to improve the guidance of interventional cardiac procedures, thereby increasing the efficiency and efficacy of those procedures.

II. Methods

A. Mechanical Design

Fig. 3 shows a schematic [Fig. 3(a)] and photograph [Fig. 3(b)] of the intracardiac ultrasound prototype. The transducer/actuator assembly was fabricated by mounting a 1.75 mm by 1.75 mm, 20 MHz PZT 5A piston onto a 75-μm thick, 2-mm square piece of gold-plated polyimide with silver conductive epoxy (Chomerics, Woburn, MA). Two 1.5-mm wide, 1.0-mm long, 3-μm thick gold-plated polyimide films were attached to a 150-μm thick, copper-plated polyimide support. The gold thickness on the films was 0.2 μm. These films then were spread apart, and the transducer and table were mounted onto the films using a thin layer of 5-minute epoxy (Hardman, Belleville, NJ). The two gold-plated films served as both the hinges upon which the table pivots and the electrical connections to the transducer. Two 4 μm silver ribbons (Sigmund Cohn, Mt. Vernon, NY) and silver epoxy were then used to make the connections from the transducer to the hinges. After the

transducer assembly was completed, the IFA was attached to the side of the polyimide table using water-soluble glue (Prang, Maitland, FL). This glue provided a secure attachment in the imaging fluid, but it allowed for easy removal of the actuator in water. The probe then was immersed in a small tube filled with HFE-7100 (3M, St. Paul, MN), a low-viscosity electrically insulating fluid, for acoustical conduction and to insulate the IFA when high voltages are applied.

In Fig. 3 the actuator is attached to only one side of the transducer table. The actuator is able to pull on only one edge of the table, deflecting the ultrasound beam in one direction from the center. The mechanical suspension of the table was designed to provide the deflection of the beam in the other direction when the IFA is relaxed. The tension in the pivot flaps will cause the table to return toward the center point, and the inertia of the table/transducer assembly will carry it past the center rest position, deflecting the beam in the other direction to complete the sector scan. In tests done with the structure moving in air, the deflection of the structure appeared to be equal in both directions with only one actuator needed. Future probe designs include an actuator on both sides of the table being alternately powered to pull on both sides of the table. Two actuators may provide a more controlled and repeatable motion of the structure.

The linear actuator used to tilt the transducer, the IFA, will be discussed in more detail. The IFAs have been described in previous publications [12–15]. These devices are patterned on 2.2 μm thick polyimide films using standard integrated circuit photolithography. IFAs were developed and are fabricated at MCNC. The fabrication is done with a two-mask process using reactive ion etching (RIE) and angled metal deposition. The IFAs are networks of hundreds of thousands of metallized polyimide plates, which form micron scale deformable capacitors. These flexible capacitors contract due to the electrostatic force produced when a differential voltage is applied across the plates. The power consumption of these devices is < 10 mW as current flows through the device only during contraction [12]. The entire IFA structure consists of three columns of networked cells and is 3-mm wide and 1-cm long with an active length of 8 mm. Each individual capacitive cell is 30-μm wide, 2.2-μm thick, and has an air gap between the plates of 1.7 μm. The schematics in Fig. 4 represent a portion of the network of the IFA cells and a single cell in both relaxed and contracted positions. The individual cells are organized into a brick-like pattern [Fig. 4(a)] to maximize both the force produced by the device and its strain.

B. Mechanical Analysis

When a differential voltage is applied across the capacitive cells of the IFA, the structure contracts in its length dimension. This force can be determined via the electrostatic force equation adjusted for the situation in which there are two dielectrics between the metal plates, polyimide, and HFE 7100 which is,

$$Force = \frac{\varepsilon A V^2}{4.4 L^2} \tag{1}$$

where ε is the dielectric constant of the material between the plates (HFE 7100, $\varepsilon = 7.39\varepsilon_0$), A is the plate area, V is the voltage across the plates, and L is the plate separation. Because the force in (1) is proportional to the plate area and inversely proportional to the square of the plate separation, the capacitive cells can be scaled down in size and still produce the same forces as a larger cell. This allows the use of many small capacitors to maximize the force per actuator area. These IFAs have been driven at frequencies up to 20 KHz and voltage of up to ± 65 [14]. For our imaging purposes, the IFAs were driven at voltages up to ± 55 Volts at drive frequencies ranging from 10–60 Hz.

In order to predict the dynamic behavior of the hinged table assembly resulting from the IFA pulling on the side of the table, it was necessary to develop models to predict the resulting motion. We modeled the device by converting the table and suspension into a simplified model of a mass and two springs. It was first assumed that the table and transducer supported on the two flexible films could be modeled as a mass suspended on the ends of two flexible cantilever beams under stress as in Fig. 5(a). After determining the equivalent linear spring constants for the two cantilevers, we converted them to linear springs to simplify the analysis. The hinged table then was modeled as a mass suspended between two linear springs as in Fig. 5(b).

The equivalent linear spring constant, k, of a cantilever beam loaded at one end is given by [16],

$$k = \frac{3EI}{l^3} \tag{2}$$

where EI is the cantilever flexural rigidity and l is the cantilever length. Jacobson [15] derived an equation to determine the flexural rigidity of a dual material beam composed of gold-plated polyimide using the method of transformed sections. This method determines an equivalent single material beam by replacing the metal layer with a polyimide layer scaled by the ratio of the elastic modulus of the metal to the elastic modulus of the polyimide to create a single material beam with bending properties equivalent to the dual material beam. Assuming that the centroid of the system is located in the gold, which is indeed the case for these hinges, EI of the equivalent beam can be determined using:

$$\begin{aligned} EI =& \frac{t_{met} d_{met}^3 E_{met}}{12} + \frac{t_{pi} d_{pi}^3 E_{pi}}{12} + \frac{d_{met}}{t_{met} E_{met}} \left(\frac{t_{pi} d_{pi} E_{pi}}{2} \right)^2 \\ &= + E_{pi} t_{pi} d_{pi} \times \\ &\left(\frac{t_{met} d_{pi} E_{met} + t_{met} d_{met} E_{met} - t_{pi} d_{pi} E_{pi}}{2 t_{met} E_{met}} \right)^2 \end{aligned} \tag{3}$$

where d_{met} is the gold thickness, t_{met} is the beam width, E_{met} is the elastic modulus of the gold, d_{pi} is the polyimide thickness, t_{pi} is the beam width, and E_{pi} is the elastic

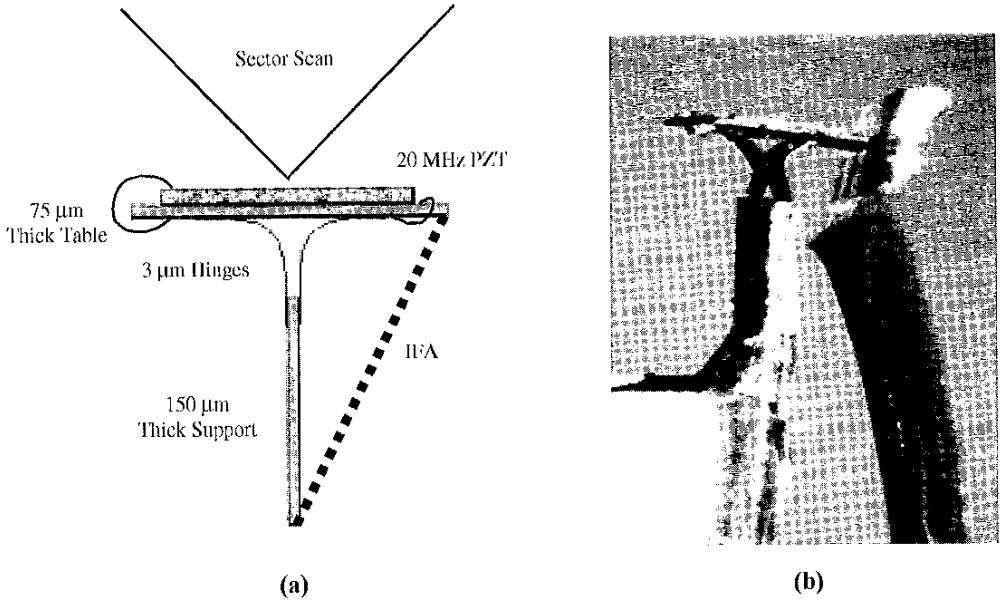

Fig. 3. IFA/transducer assembly for the forward looking device. (a) Schematic of device, (b) Photograph of early prototype.

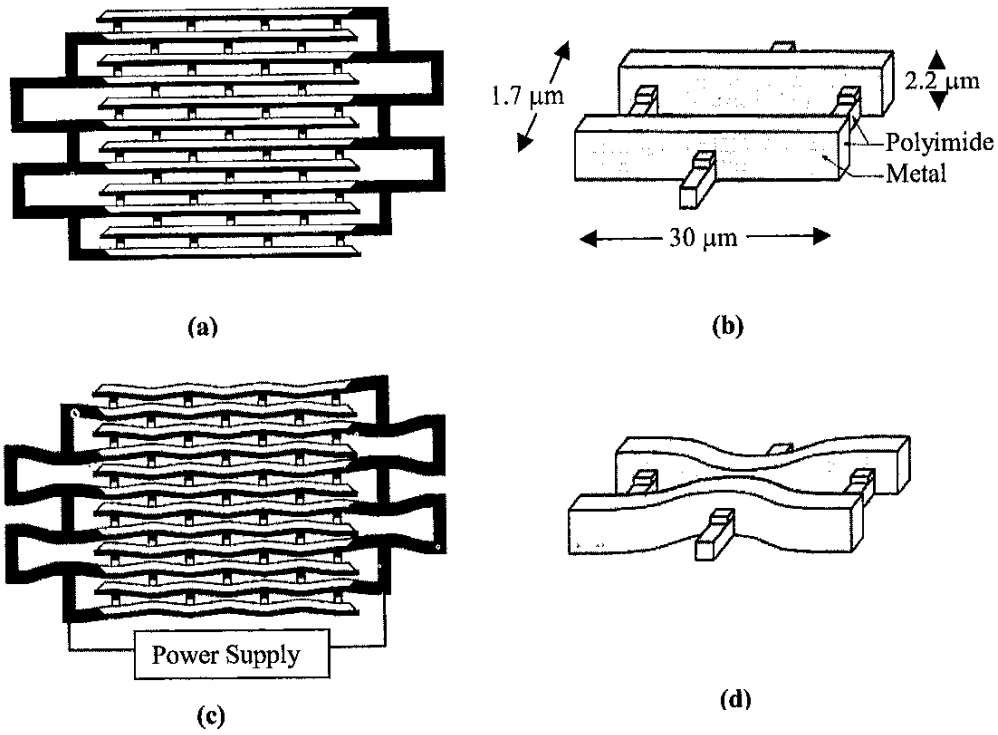

Fig. 4. Schematics of the integrated force array. (a) A group of cells in the array, (b) a close-up of a single capacitive cell, (c) contraction of the cells in the array, and (d) contraction of a single capacitive cell.

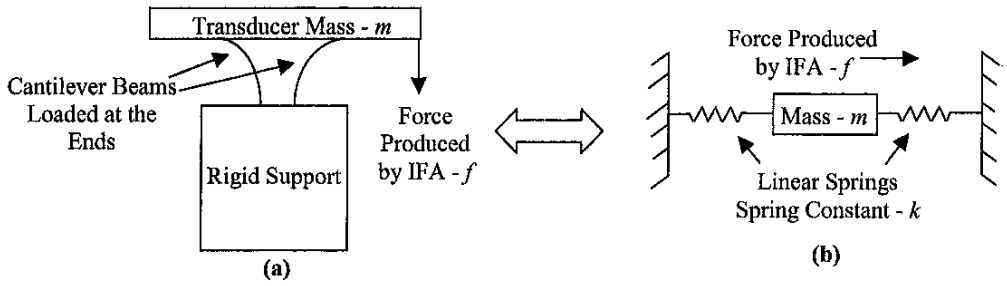

Fig. 5. Schematics of models for hinged table assembly: (a) model as built; (b) reduced one-dimensional model.

modulus of the polyimide. Using the dimensions of the prototype hinges and the elastic moduli of gold ($77.2 * 10^9$ N/m^2) and polyimide ($2.6 * 10^9$ N/m^2), the EI of the beam was determined to be $3.7 * 10^{-11}$ Nm^2. (2) then was used along with the length of the cantilevers, $l = 1.0$ mm, to determine an effective linear spring constant, k, for the cantilevers of .1110 N/m.

Using the model from Fig. 5(b), it was possible to determine a differential equation describing the motion in the x dimension of the mass when a force is applied by setting the forces acting on the mass equal to each other:

$$f = m\frac{dx^2}{dt^2} + 2kx. \tag{4}$$

Using a Laplace transform of the homogeneous solution to (4), it is possible to determine the transfer function H with respect to the complex frequency s for the suspension:

$$H(s) = \frac{1}{ms^2 + 2k}. \tag{5}$$

This transfer function leads to a characteristic equation of:

$$ms^2 + 2k = 0. \tag{6}$$

This characteristic equation results in the prediction of a single resonance frequency for the unforced structure given by:

$$f = \frac{1}{2\pi}\sqrt{\frac{2k}{m}} \tag{7}$$

where k is the effective linear spring constant of each of the springs and m is the mass of the transducer and table. By using values for the calculated $k = .1110$ N/m and the measured mass of an assembled table and transducer, $m = 2$ mg, for the prototype structure, we calculated the theoretical resonance to occur at 53.0 Hz. Immersing the structure into the insulating fluid would be expected to dampen the motion of the structure and would be represented by a dash pot in parallel with each of the springs in the model of Fig. 5(b). The resonance of the structure in the fluid would be expected to occur at a lower frequency. In a future paper, the modeling of these structures will be carried out further using finite element simulations to more accurately predict the structure's motion.

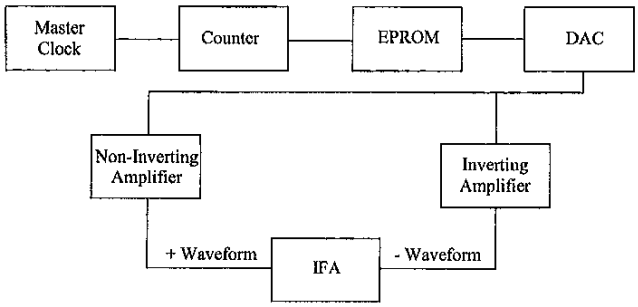

Fig. 6. Block diagram of IFA differential driving circuitry.

C. Electronic Design

Circuitry was designed to supply a differential drive voltage to the IFA and to trigger the imaging circuitry for the ultrasound transducer. A block diagram of the IFA drive circuitry is shown in Fig. 6. The drive system consists of a master clock incrementing a 7-bit counter that cycles through a lookup table of 128 voltage values in an EPROM that is converted by a digital to analog converter (DAC) to produce a triangle voltage wave output. This triangle wave then is passed through two high-power operational amplifiers (Model 3584JM, Burr-Brown, Chicago, IL) set up in inverting and noninverting configurations to produce a high voltage positive wave and a high voltage negative wave. This results in two triangle waves that are exactly 180°out of phase with each other. These two high voltage waveforms are used to apply an oscillating differential voltage across the capacitor cells in the IFA. The master clock that drives the IFA circuitry also is divided by two and used to trigger the imaging circuitry to keep the entire system synchronized and to ensure that the imaging lines are acquired at the same point in each sectoring motion of the IFA.

A block diagram of the imaging system used to obtain the ultrasound data is shown in Fig. 7. The master clock from the IFA driving circuitry was divided by two and used as the trigger pulse for both the pulser and the signal acquisition circuitry. The transducer was pulsed 64 times for each contraction and expansion cycle of the IFA in order to generate a 64 line image for each sweep of the transducer. The ultrasound lines then were fed into an imaging system based on a personal computer. A Hewlett Packard

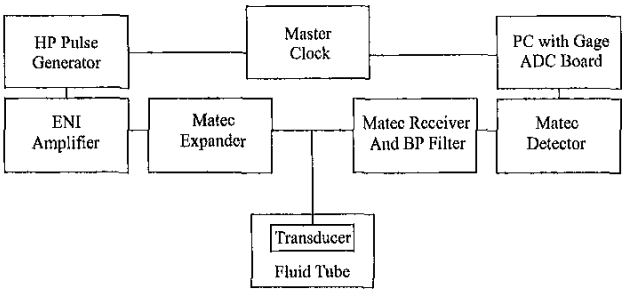

Fig. 7. Block diagram of digital imaging system.

8165A Programmable Signal Source in conjunction with a Model 325L RF Power Amplifier (ENI, Rochester, NY) was used to provide a bipolar, two-cycle sinusoidal pulse with a peak-to-peak amplitude of 50 volts to the transducer. Following Lockwood *et al.* [17], an expander (Matec, Northborough, MA) was placed in series with the pulser to eliminate it from the circuit in receive mode. A t-junction was used to drive the transducer and carry echoes to the receive portion of the circuitry. The received echoes were passed through a Model 625 Broadband Receiver (Matec, Northborough, MA), which amplified the signals before they were passed through a band pass filter centered at 21.4 MHz (Mini-Circuits, Deer Park, NY). The Matec receiver was used to envelope detect the filtered signals. The RF detected signals from the receiver were fed into an 8012A Compuscope (Gage, South Burlington, VT) analog to digital conversion board operating at 100 MSamples/Sec that is housed in a personal computer. The digitized data lines were assembled using LabVIEW software (National Instruments, Austin, TX) to generate real-time B-mode images with frame rates of 10 Hz. This rate is limited only by the software and could be increased if necessary by optimizing the code.

D. Transducer Design

The transducer was modeled using PiezoCAD Software (Sonic Concepts, Woodinville, WA), which uses the one-dimensional KLM equivalent circuit model. The simulated results were used in order to optimize the area of the transducer for maximum power transfer from the pulser to the transducer and to predict the complex impedance and the pulse-echo response of the transducer. The material properties entered into the software model are contained in Table I. For this early prototype transducer, no matching layer or electrical matching network was used. The model simulated the prototype transducer that we built immersed in an HFE 7100 medium.

In addition, this transducer also was analyzed using standard diffraction theory to evaluate its expected beam characteristics. For the 1.75-mm wide aperture with an operating frequency of 20 MHz, the far-field transition point will occur at approximately 1 cm, and the resolution at that point will be 0.44 mm.

E. Transducer and System Evaluation

The following experiments were conducted with the transducer/IFA assembly and the imaging system described. The vector impedance plot of the transducer was measured and compared to results simulated using PiezoCAD. The pulse-echo waveforms and frequency spectra of the table transducer then were obtained after reflection off of a polished aluminum block and compared to simulations. In addition, the 50Ω pulse-echo insertion loss of the table transducer was measured as described by Sherar and Foster [18]. The transducer/IFA assembly then was used to image a wire phantom that consisted of a group of wires arranged in a V pattern. The wires were spaced 2 mm apart in depth and 0.5 mm apart laterally for a total width of 9 mm at the bottom of the phantom to produce an angle in the phantom of ±14°. For these preliminary images, no $r,\theta \rightarrow x,y$ scan conversion for the mechanical sector scanner was performed. The detected RF lines were placed in a rectangular matrix and displayed as an intensity plot.

III. Results

In Section II-B, a simplified model of the hinged transducer assembly that modeled the structure as a mass suspended between two springs was developed. This model and the equations derived from it predicted a resonant frequency of the structure at 53.0 Hz. In experiments done with the IFA/transducer assembly driven in air, a single resonance of the structure was visualized using a microscope with a calibrated graticule. This resonance occurred at a frequency of 56 Hz, which agrees well with the resonance frequency predicted by the mass and spring model. The discrepancies between the two values could be due to the fact that the IFA attached to the table also will affect the mechanical resonance of the structure.

Fig. 8 shows simulated and measured vector impedance plots of the table-mounted transducer immersed in the HFE-7100 fluid. The simulated and measured magnitude plots agree well with each other in amplitude and location of the parallel resonance peak. The phases of the simulated and measured impedance plots differ quite a bit though. The differences between the simulated and measured results are most likely due to the fact that the model is only one-dimensional, and the actual device is three-dimensional. A two- or three-dimensional finite element model may be necessary to get better agreement. The plots show that the parallel resonance of the PZT in both the measured and simulated waveforms occurs at about 23 MHz. In addition, the magnitude of the impedance at the PZT resonance frequency is close to 50 Ohms, so the power transfer from the 50 Ohm drive circuitry to the transducer should be efficient.

The simulated and measured pulse-echo responses and the corresponding power spectra are shown in Fig. 9. The measured −6 dB and −20 dB pulse lengths of the

TABLE I
PIEZOCAD MATERIAL PARAMETERS.

Material	Thickness	Acoustic impedance	Sound velocity
PZT 5A	101.3 μm	37 MRayls	4660 m/sec
Silver epoxy	20 μm	5.1 MRayls	1900 m/sec
Gold plating	.2 μm	63.828 MRayls	3240 m/sec
Polyimide	77.8 μm	3.1 MRayls	2200 m/sec
Hardman epoxy	.2 μm	2.86 MRayls	2600 m/sec
HFE 7100	infinite	1.025 MRayls	674.67 m/sec

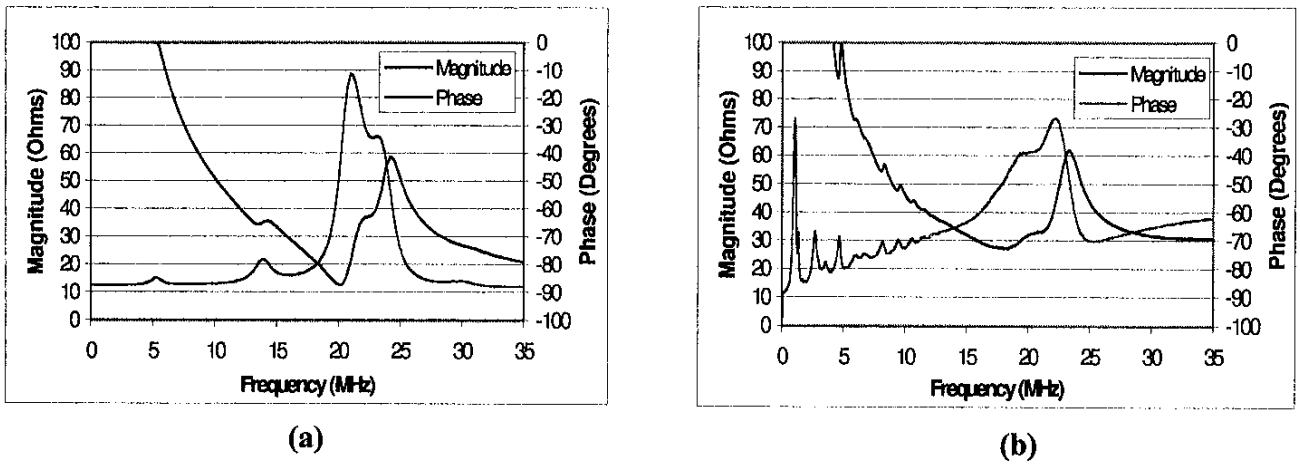

Fig. 8. Impedance plots of table-mounted transducer immersed in HFE 7100 fluid. (a) Simulated, and (b) measured.

transducer were 0.25 μsec and 0.5 μsec, respectively, compared to 0.16 μsec and 0.48 μsec for the simulated pulse. The measured -6 dB bandwidth of the transducer was 25.2%, and the simulated -6 dB bandwidth was 25.3%. The simulated pulse and power spectrum are in reasonable agreement with the measured results. These simulations most likely would agree better if the simulation were done in more dimensions than the one-dimensional KLM model. The 50Ω pulse-echo insertion loss of the transducer was measured as -32 dB. This is slightly higher than the -26 dB reported by Lockwood *et al.* [19] for a single-element, high-frequency transducer, but it is expected due to the lack of an acoustic matching layer and electrical matching network on this early prototype transducer. However, this insertion loss compares well with that reported by Sherar and Foster [18] for a high frequency PVDF transducer, -35 dB, and is less than that reported by Lucacs *et al.* [20] for a single element PZT sol gel transducer, -46 dB.

Fig. 10 compares a map of a wire phantom used to evaluate the performance of our prototype [Fig. 10(a)] with a B-mode image of the phantom acquired using the developed probe. Fig. 1(b) is a representative still from the real-time image obtained by powering the IFA to tilt the transducer and sector the beam across the phantom. In the image, seven wires in depth are visible when the transducer is 3 cm from the top of the wire phantom. The second two wires are barely resolved at this distance. These results are expected because those two wires are 1 mm apart, and at 3 cm we expect a beam width of 1.2 mm. By utilizing the known depth information and the number of wires on each side of the phantom that are visible to the probe, we were able to estimate that a sector angle of approximately $\pm 5^\circ$ was achieved in this image. Previous images of other phantoms have led to sector scan estimates up to $\pm 10^\circ$.

IV. DISCUSSION

We have developed an early prototype of a forward-looking intracardiac ultrasound probe that might improve the guidance of interventional cardiac procedures. The PZT transducer and the MEMS actuator that make up the key components of the device were investigated and described in detail. The prototype device was interfaced with a single-channel high frequency scanner using a personal computer platform. This imaging system was used to produce real time B-scan images. This new single-channel scanner might have distinct advantages over conventional technologies. With the proper design, the entire actuator and mechanical assembly could be fabricated using conventional integrated circuit photolithography, thereby greatly decreasing its eventual cost. Also, only four connection wires, two for the differential powering of the IFA and two for the ultrasound element, are necessary to power the device. Therefore, the catheter could remain small and flexible and would be able to traverse the necessary bends easily as it is advanced into the heart.

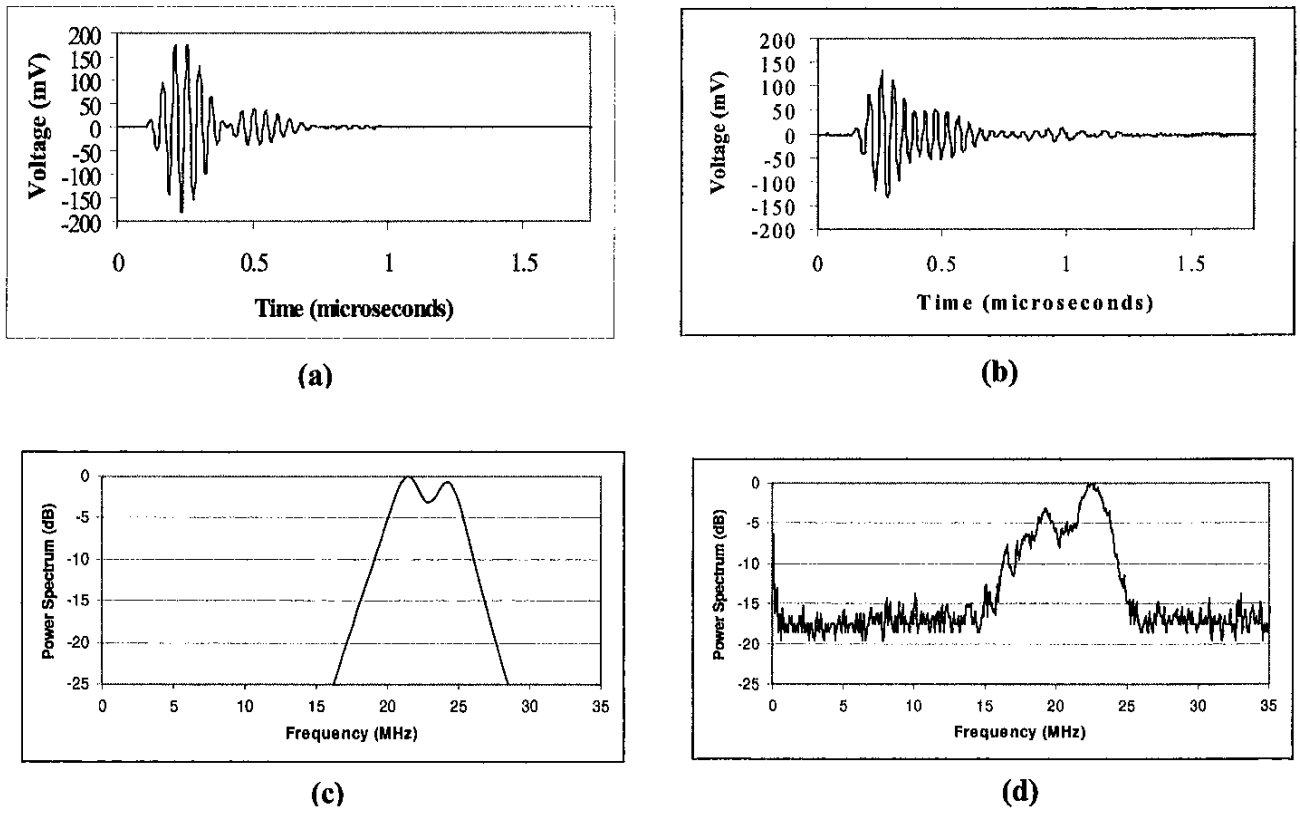

Fig. 9. (a) Simulated pulse-echo response of table transducer, (b) measured pulse-echo response of table transducer, (c) simulated power spectrum of transducer, and (d) measured power spectrum of transducer.

The necessary imaging capabilities of catheter ultrasound probes will vary depending on the design constraints for specific intracardiac imaging tasks. The principle tradeoff is the goal of achieving the highest transducer frequency to improve spatial resolution versus the need for adequate sensitivity and tissue penetration. We believe the probe we have designed, which operates at 20 MHz, will offer advantages for the guidance of procedures requiring imaging of the endocardial surface due to its lateral resolution of 0.44 mm with tissue penetrations up to 1 cm. This resolution should be more than adequate for imaging the fossa ovalis or the pulmonary veins as well as imaging RF ablation procedures. As was shown in Fig. 1, the depth of penetration in heart tissue at 20 MHz is approximately 6–7 mm.

However, in procedures such as left ventricular monitoring from the right ventricle, which require the ultrasound beam to penetrate the septum, this penetration depth may not be sufficient, and lower frequency transducers (10 MHz or lower) may be more appropriate. For these types of applications, a total scan depth of 10 cm may be necessary. A significant advantage of our design is that, in order to change the imaging frequency, only the piezoelectric element needs to be changed, with very little need to redesign other aspects of the system. This allows our probe to be modified to fit the needs of each individual application.

These initial results are very encouraging, but several areas need improvement in order to produce a clinically viable catheter scanner. The deflection of the transducer needs to be increased from the current sector angle of ±5° to ±30° to produce a more clinically useful sector scan. This could be accomplished by developing integrated force arrays that are fabricated from polyimide films which are twice as thick (4.4 μm) as the current devices (2.2 μm). According to (1), this would double the force produced by the actuators and should, in turn, increase the deflection of the ultrasound beam. A new fabrication run of custom actuators is currently under way to approach this issue. In addition, efforts are underway to maximize the flexibility of the hinge structure in order to minimize the force required to tilt the transducer.

The new actuator design also will produce other IFA devices that are only 1-mm wide compared to 3-mm wide for the current generation of devices. These devices will consist of only one column of networked cells, which will decrease the force produced by the actuator but will not affect the strain produced. It is not clear at this point if the motion of the table is force limited or strain limited, so the motion of the transducer that will result from these new 1 mm IFAs remains to be determined. Currently, the limiting factor in the miniaturization of the probe is the width of the IFA. Reducing the width of the IFA will allow for the entire probe to be made smaller to allow for insertion of the device into a smaller catheter sheath. Our current

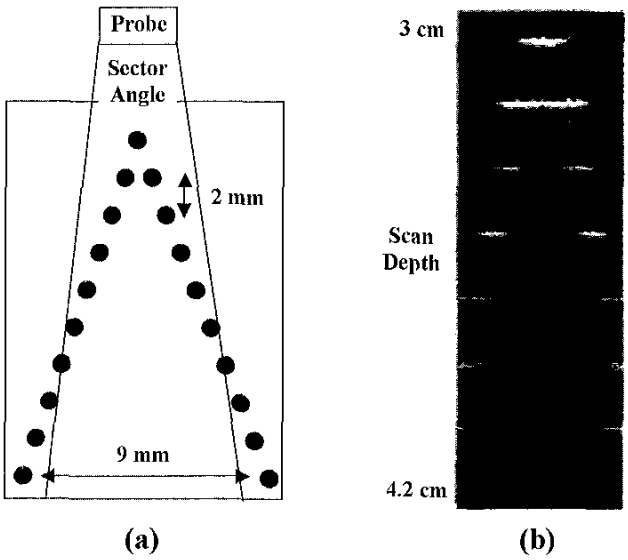

Fig. 10. Off-line images made with digital imaging system with 20 MHz transducer. (a) Map of wire phantom, and (b) still from real-time image of wire phantom.

prototype would require a 12 French (O.D. = 3.82 mm) catheter to house it, and a probe built with a 1-mm wide IFA could be placed into a 9 French (O.D. = 2.86 mm) catheter. This would increase the number of possible uses for the probe.

Another area to be addressed is to improve the performance of the transducer and the imaging system. An acoustic matching layer will be added to the transducer to decrease its pulse length, broaden its bandwidth, and decrease its insertion loss. A thin layer of polyimide over the front of the transducer has been identified as a suitable matching layer. We fabricated similar transducers on rigid supports with polyimide matching layers, which showed an increased bandwidth (46%) and a +5dB increase in the received pulse amplitude [21]. Transducers mounted on flexible hinges with polyimide matching layers are currently under development.

One additional step toward a viable clinical probe would be to encase the transducer/IFA assembly in a fluid-filled catheter sheath. The catheter sheath will be designed with an acoustic window at the tip for sound conduction. This catheter sheath also initially will be filled with HFE-7100 fluid in order to insulate the voltages on the integrated force array and for sound coupling from the transducer to the blood in the heart. Due to concerns about the biocompatibility of HFE-7100, we are working on using a thin film of parylene polymer to insulate the IFA from the environment, which would enable us to use saline to fill the catheter tube. To increase the effectiveness of the probe, it will be necessary to have a mechanism to steer the catheter itself in order to obtain the desired fields of view within the heart. This could be achieved by using either steering wires within the catheter sheath or a catheter sheath that is steerable. After these improvements are made, the transducer could be used to image cardiac phantoms. For example, we have developed flexible excised animal hearts contained in a hydraulic pumping chamber that uses fluid pressure to produce a passively beating heart for imaging purposes [22]. We also could proceed on to conducting animal trials and clinical evaluation of the probe.

Another area for future experimentation is the development and evaluation of analytical models to evaluate the expected motions of the IFA and mechanical suspension. This analysis was begun with the simple model described previously. The simple formulation presented only predicts a resonance frequency and does not take into account the motion and weight of the IFA attached to the polyimide table. In order to determine the dynamic behavior of the table/IFA system, finite element simulations will be necessary. These simulations also will give a better idea of the motion and speed of the table, as it is changing direction in its sector, and allow us to perform accurate scan conversion to compensate for the varying speeds of the transducer in the course of its motion.

Acknowledgments

We wish to thank Professor Richard Fair for his valuable discussions on the original design of the micromachine scanner. We wish to thank P. Wolf, J. Castelucci, R. Gupta, and E. Light for helpful conversations.

References

[1] N. Bom, C. T. Lancee, and F. C. Van Egmond, "An ultrasonic intracardiac scanner," *Ultrasonics*, vol. 10, pp. 72–76, 1972.

[2] P.G. Yock, E. Johnson, and D. Linker, "Intravascular ultrasound: Development and clinical potential," *Amer. J. Cardiac Imaging*, vol. 2, pp. 185–193, 1988.

[3] P. Yock, P. Fitzgerald, and R. Popp, "Intravascular ultrasound," *Sci. Amer. Sci. Med.*, pp. 68–77, Sept./Oct. 1995.

[4] D. H. Liang and B. S. Hu, "A forward-viewing intravascular ultrasound catheter suitable for intracoronary use," *Biomed. Instru. Tech.*, pp. 45–53, 1997.

[5] J. L. Evans, K. Ng, M. J. Vonesh, B. L. Kramer, S. N. Meyers, T. A. Mills, B. J. Kane, W. N. Aldrich, Y. Jang, P. G. Yock, M. D. Rold, S. I. Roth, and D. D. McPherson, "Arterial imaging with a new forward-viewing intravascular ultrasound catheter. I, Initial studies," *Circulation*, vol. 89, pp. 712–723, 1994.

[6] N. G. Pandian, S. L. Schwartz, A. R. Weintraub, T. L. Hsu, M. A. Konstam, and D. N. Salem, "Intracardiac echocardiography: Current developments," *Int. J. Cardiac Imaging*, vol. 6, pp. 207–219, 1991.

[7] J. B. Seward, D. L. Packer, R. C. Chan, M. Curley, and A. J. Tajik, "Ultrasound cardioscopy: Embarking on a new journey," in *Mayo Clin. Proc.*, vol. 71, pp. 629–635, 1996.

[8] E. D. Light, R. E. Davidson, J. O. Fiering, T. A. Hruschka, and S. W. Smith, "Progress in two-dimensional arrays for real-time volumetric imaging," *Ultrason. Imaging*, vol. 20, pp. 1–15, 1998.

[9] E. D. Light, J. O. Fiering, W. Lee, P. D. Wolf, and S. W. Smith, "Two-dimensional catheter arrays for real time intracardiac volumetric imaging," in *Proceedings of SPIE, Medical Imaging 1999: Ultrasonic Transducer Engineering*, K. Kirk Shung, Ed. vol. 3664, pp. 76–84, 1999.

[10] C. Stellbrink, J. Siebels, J. Hebe, D. Koschyk, G. Haltern, K. Ziegert, P. Hanrath, and K. Kuck, "Potential of intracardiac ultrasonography as an adjunct for mapping and ablation," *Amer. Heart J.*, pp. 1095–1101, Apr. 1994.

[11] J. M. Kalman, J. Juc, S. Krishnankutty, P. Fitzgerald, P. Yock, and M. D. Lesh, "In vitro quantification of radiofrequency ablation lesion size using intracardiac echocardiography in dogs," *Amer. J. Cardiol.*, vol. 77, pp. 217–219, 1996.
[12] S. M. Bobbio, M. D. Kellam, B. W. Dudley, S. Goodwin-Johansson, S. K. Jones, J. D. Jacobsen, F. M. Tranjan, and T. D. Dubois, "Integrated force arrays," in *Proc. of the IEEE Micro Electro Mechanical Systems Workshop*, Ft. Lauderdale, FL, pp. 149–155, IEEE, Feb., 1993.
[13] S. Bobbio, S. Goodwin-Johansson, T. DuBois, F. Tranjan, S. Smith, R. Fair, C. Ball, J. Jacobsen, C. Bartlett, N. Eleyan, H. Makki, and R. Gupta, "Integrated force array: Positioning drive applications," *SPIE*, vol. 2722, pp. 123–134, 1996.
[14] S. M. Bobbio, S. W. Smith, S. Goodwin-Johansson, R. B. Fair, T. D. DuBois, F. M. Tranjan, J. Hudak, R. Gupta, and H. Makki, "Integrated force array: Interface to external systems," *SPIE*, vol. 3046, pp. 248–259, 1997.
[15] J. Jacobson, "Integrated force arrays: Theory, modeling, fabrication, analysis and feasibility study," Ph.D. Dissertation, Duke Univ., Durham, NC, 1995.
[16] J. E. Shigley and C. R. Mischke, *Mechanical Engineering Design*. 5 ed. New York: McGraw-Hill, 1989, pp. 106–108.
[17] G. R. Lockwood, J. W. Hunt, and F. S. Foster, "The design of protection circuitry for high frequency ultrasound imaging systems," *IEEE Tran. Ultrason., Ferroelec., Freq. Contr.*, vol. 38, no. 1, pp. 48–55, 1991.
[18] M. D. Sherar and F. S. Foster, "The design and fabrication of high frequency poly(vinylidene fluoride) transducers," *Ultrason. Imaging*, vol. 11, pp. 75–94, 1989.
[19] G. R. Lockwood, D. H. Turnbull, and F. S. Foster, "Fabrication of high frequency spherically shaped ceramic transducers," *IEEE Trans. Ultrason., Ferroelec., Freq. Contr.*, vol. 41, no. 2, pp. 231–235, 1994.
[20] M. Lucaes, M. Sayer, and S. Foster, "Single element and linear array PZT ultrasound biomicroscopy transducers," in *Proc. IEEE Ultrason. Symp.*, pp. 1709–1712, 1997.
[21] J. M. Zara, S. Bobbio, R. Fair, S. Goodwin-Johansson, and S. W. Smith, "A forward looking intracardiac ultrasound scanner using MEMS technology," in *1998 ONR Transducer Materials and Transducers Workshop*, Penn State Univ., State College, PA, May 12–14 1998.
[22] S. W. Smith, P. D. Lopath, D. B. Adams, and G. P. Walcott, "Cardiac ultrasound phantom using a porcine heart model," *Ultrasound Med. Biol.*, vol. 21, no. 5, pp. 693–697, 1995.

Jason M. Zara was born in Peoria, IL on June 24, 1974. He received a B.S. degree in Bioengineering from the University of Illinois at Urbana-Champaign in 1996. He is currently pursuing a Ph.D. degree in biomedical engineering at Duke University and is being supported by a Whitaker Foundation graduate fellowship. His current research concerns the use of MEMS technology in the design and development of an intracardiac ultrasound scanner.

Stephen M. Bobbio is currently Professor of Electrical Engineering at the University of North Carolina at Charlotte. He received a Ph.D. in Physics from the College of William and Mary, and, for the past 20 years, he has been active in the areas of microelectronics and microstructures. He has published 60 papers and has had 26 issued patents. He is currently a member of the SPIE program committee for Smart Electronics and MEMS.

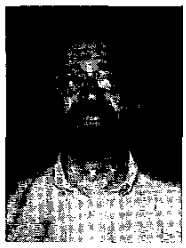

Scott H. Goodwin-Johansson (S'79–M'79 M'80–S'80–M'83) received the B.S. degree in Electrical Engineering in 1979 and the M. Eng. degree in 1980 from Rensselaer Polytechnic Institute, Troy, NY. He was supported by the IEEE Fortescue Fellowship during his studies for the M. Eng. degree. He received the Ph.D. degree in Electrical Engineering from Stanford University, Stanford, CA, in 1984 and was supported by a Hertz Foundation Fellowship. His thesis investigated the device physics of isolation structures.

Since 1984, he has been a member of the Technical Staff at the Materials and Electronic Technologies Division of MCNC. For the past 9 years, he has been involved in the MEMS activities at MCNC, developing the IFA and other MEMS structures and actuators. Previous work involved the device and process design of one micron and submicron CMOS technologies, including two-dimensional doping profile measurements.

Dr. Goodwin-Johansson is a member of Tau Beta Pi and Eta Kappa Nu.

Stephen W. Smith (M'91) was born in Covington, KY, on July 27, 1947. He received the BA degree in physics in 1967 from Thomas More College, Ft. Mitchell, KY; the MS degree in physics in 1969 from Iowa State University, Ames; and the Ph.D. degree in biomedical engineering in 1975 from Duke University, Durham, NC.

In 1969, he became a Commissioned Officer in the U.S. Public Health Service, assigned to the Food and Drug Administration, Center for Devices and Radiological Health, Rockville, MD, where he worked until 1990 in the study of medical imaging, particularly diagnostic ultrasound and in the development of performance standards for such equipment. In 1978, he became an adjunct Associate Professor of Radiology at Duke University Medical Center. In 1990, he became Associate Professor of Biomedical Engineering and Radiology and Director of Undergraduate Studies in Biomedical Engineering at Duke University. He holds seven patents in medical ultrasound and has authored 100+ publications in the field.

Dr. Smith has served on the education committee of the American Institute of Ultrasound in Medicine, the executive board of the American Registry of Diagnostic Medical Sonographers, and the editorial board of *Ultrasonic Imaging*. He was co-recipient of the American Institute of Ultrasound in Medicine Matzuk Award in 1988 and 1990 and co-recipient of the IEEE-UFFC Outstanding Paper Award in 1983 and 1994.